International Journal of Control and Automation
Vol.7, No.7 (2014), pp. 179-190
http://dx.doi.org/10.14257/ijca.2014.7.7.15

Electric Field Finite Element Analysis and Experimentation of Plate-Plate Type Electrospinning Machine

Duan Hong-wei[1, 2], Jiang Jin-gang[1]*, Li Bo-yang[1], Li Bin[1] and He Tian-hua[1]

[1]*Intelligent Machine Institute, Harbin University of Science and Technology, Heilongjiang Harbin 150080, China*
[2]*School of Material Science and Engineering, Harbin University of Science and Technology, Harbin 150040, China*
**jiangjingang1982@163.com*

Abstract

The analysis of electric field distribution in electrospinning machine is critical to the nanofiber preparation. In this paper, electric field strength is calculated based on finite element calculation theory of electric field. Electric field structure of plate-plate type electrospinning machine is simulated using ANSYS software. And vector distribution of nozzle on spinneret pipe of plate-plate type electrospinning machine is obtained. The simulation analysis provides an effective reference for the electric field's distribution of the plate-plate type electrospinning machine. Based on the experimental system of the plate-plate type electrospinning machine, electrospinning experiment with different spinning distance and extrusion speed is performed. The experimentation results show that fiber diameter decreases with the increase of spinning distance, and the extrusion speed and the diameter of the fiber conform to the direct proportion.

Keywords: *electric field, finite element analysis, plate-plate type, electrospinning machine*

1. Introduction

Electrospinning technique is currently one of the most important methods for preparing. It is important and essential to analyze the electric field distribution in electrospinning machine. The polymer solutions or melts with charge flow and deform at strong static electric field, and solvent is evaporated or the melt is cooled and solidified, then fibroid substance is obtained. In high electric field, fluid is ejected from Taylor core and formed jet flow. Jet flow with electricity speed up and its diameter becomes tiny in the electric field [1-3]. This is the reason that electrospinning can obtain the nanofibre. Figure 1 is schematic diagram of electrospinning device [4]. In essence, electrostatic force is unique driving force in electrospinning. So, whether the distribution of electric field is reasonable will direct affect the fineness and morphology of electrospinning fibre. The fluidic instability phenomenon exist in undesired electric field distribution, especially in sudden drop of field intensity, this will lead to uncertainty of jet flow in the receiver. Unordered diffusion in the process of electrospinning exisits with external disturbance [5]. This not only pollute experimental environment, but also waste experimental material and reduce the efficiency of electrospinning. The fluidic instability phenomenon can be weakened by controlling the shape and the strength of macroscopic electric field based on the analysis of Reneker's electrostatic spinning process [6-7]. Consequently, it is important and essential to analyze the distribution of electric field in electrospinning machine.

ISSN: 2005-4297 IJCA

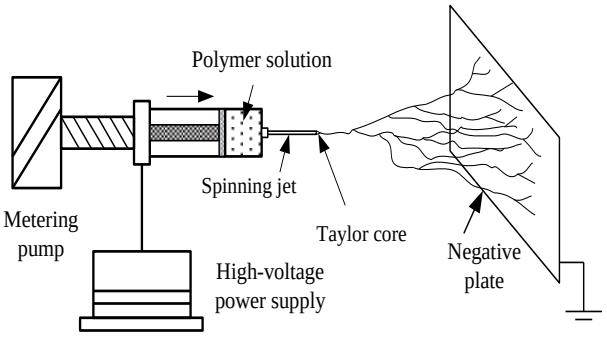

Figure 1 Electrospinning Device

2. Finite Element Calculation theory of Electric Field

2.1. The Potential Function φ

Suppose the potential function φ of each small unit *e* is the linear function of *r* and *z*, so the electric filed is regarded as a homogeneous one approximately in each small unit domain. Thus every point's potential of each unit meet the following potential interpolation function.

$$\varphi = \alpha_1 + \alpha_2 r + \alpha_3 z \tag{1}$$

Aiming to one single unit, suppose its three node number respectively is i, j, and m (counterclockwise arranging), the function of the start point i should meet Equation (1).

$$\begin{cases} \varphi_i = \alpha_1 + \alpha_2 r_i + \alpha_3 z_i \\ \varphi_j = \alpha_1 + \alpha_2 r_j + \alpha_3 z_j \\ \varphi_m = \alpha_1 + \alpha_2 r_m + \alpha_3 z_m \end{cases} \tag{2}$$

$$\begin{cases} \alpha_1 = \dfrac{1}{2S_e}\left(\alpha_i\varphi_i + \alpha_j\varphi_j + \alpha_m\varphi_m\right) \\ \alpha_2 = \dfrac{1}{2S_e}\left(b_i\varphi_i + b_j\varphi_j + b_m\varphi_m\right) \\ \alpha_3 = \dfrac{1}{2S_e}\left(c_i\varphi_i + c_j\varphi_j + c_m\varphi_m\right) \end{cases} \tag{3}$$

S_e is the area of unit e:

$$S_e = \frac{1}{2}\begin{vmatrix} 1 & r_i & z_i \\ 1 & r_j & z_j \\ 1 & r_m & z_m \end{vmatrix} = \frac{1}{2}\left(b_i c_j - b_j c_i\right) \tag{4}$$

So the interpolation function of unit e is as follows.

$$\varphi(x,y) = \frac{1}{2S_e}\left[\left(a_i + b_i r + c_i z\right)\varphi_i + \left(a_j + b_j r + c_j z\right)\varphi_j + \left(a_m + b_m r + c_m z\right)\varphi_m\right] \tag{5}$$

2.2. The Energy Function of Unit *e*

The energy function of unit e is as follows.

$$W_e = \iint_e \frac{\xi_e}{2}\left[\left(\frac{\partial\varphi^3}{\partial r}+\frac{\partial\varphi^2}{\partial z}\right)\cdot 2\pi d_r d_z\right] \tag{6}$$

According to the Equation (3), we know that $\frac{\partial\varphi}{\partial r}=\alpha_2$, $\frac{\partial\varphi}{\partial z}=\alpha_3$, that is, $\frac{\partial\varphi}{\partial r}$ and $\frac{\partial\varphi}{\partial z}$ of each point in unit e are both definite value, and it is not influenced by coordinate (r,z), so W_e can be simplified.

$$W_e = \frac{\xi}{2}\cdot 2\pi\frac{\left(\sum b_s\varphi_s\right)^2+\left(\sum c_s\varphi_s\right)^2}{4S_e^2}\iint_s r d_r d_z \tag{7}$$

$$\iint_s r d_r d_z = \frac{r_i+r_j+r_m}{3}S_e = r_e S_e \tag{8}$$

Where, r_e is the distance from the center of triangle unit e to the axis z.

Thus,

$$W_e = \frac{1}{2}\cdot\frac{2\pi\xi_e r_e}{4S_e}\left[\left(\sum b_s\varphi_s\right)^2+\left(\sum c_s\varphi_s\right)^2\right] \tag{9}$$

2.3. Calculation of Electric Field Strength

Computational equation of electric field intensity is as follows.

$$\vec{E} = -\nabla\varphi = -\frac{d\varphi}{dr}\cdot\vec{e}_r - \frac{d\varphi}{dz}\cdot\vec{e}_r = E_{re}\vec{e}_r + E_{ze}\vec{e}_r \tag{10}$$

Where, $E_{re} = -\frac{\partial\varphi}{\partial r} = -\frac{1}{2S_e}\left(\sum_{s=i,j,m} b_s\varphi_s\right)$, $E_{ze} = -\frac{\partial\varphi}{\partial z} = -\frac{1}{2S_e}\left(\sum_{s=i,j,m} c_s\varphi_s\right)$.

Its absolute value is,

$$E = \sqrt{E_{re}^2+E_{ze}^2} = \sqrt{\frac{\partial\varphi}{\partial r}+\frac{\partial\varphi}{\partial z}} \tag{11}$$

3. Electric Field Structure Simulation of Plate-plate Type Electrospinning Machine

3.1. Set up and Simplification of Electric Field

In order to get better collecting result of spinning, the electric-field distribution between the spinning jet and the negative plate is the main influencing factor. Therefore, the working model of the whole electric field can be divided into 2 parts: one is the metal spinning jet, the other is negative plate. The spinning jet added high voltage static electricity is the factor that produces electric field, and the generated electrostatic field has a spatial symmetry, so we can

deal with it as 2D field [8-10]. We analyze the model by simplify it into two dimension electric field model.

Because the aperture of metal spinning jet is very tiny (ususlly 0.4mm), in order to simplify the structure of spinning jet, we separately set up the finite-element model of the model Fig. 2(a) and model Fig. 2(b), and analyze and compare the difference of simulation results. The difference between model Fig. 2(a) and model Fig. 2(b) is that model Fig. 2(a) has pore and model Fig. 2(b) is replaced in entity. The analysis result shows that there are identical voltages distribution maps of the two types of structures, as is shown in Fig 2. It indicates that the spinning jet can be completely replaced by model Fig. 2(b). And the result from structural simplify can be controlled within allowable error.

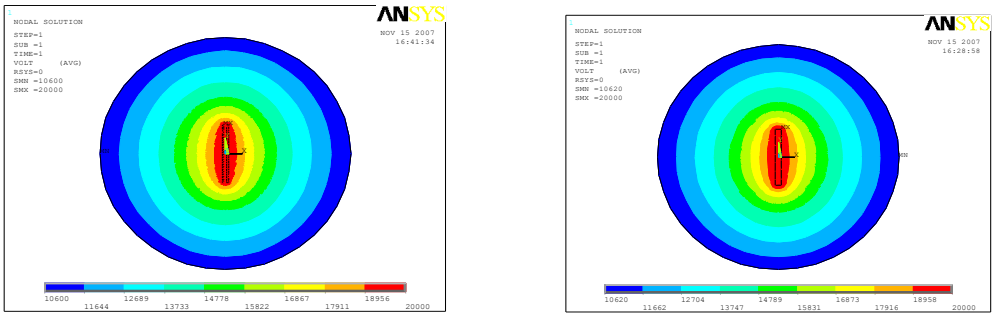

(a) Voltages distribution before simplification (b) Voltages distribution after simplification

Figure 2 Voltages Distribution Maps of Spinning Jet

3.2. FEA of Electric Field

Traditional H-method is adopted to analyze FEA of electrostatic field [11-12]. Some assumptions are proposed. 1) the dielectric constant of medium is constant and doesn't depend on electric field; 2) influences of electric charge of electrification spinning fiber was ignored; 3) effects of control elements on electric-field distribution would be neglected; 4) we supposed the volume density of field electric charge $\rho=0$. Through selecting various kinds of unit and comparing analysis results with actual data, we chose 8 nodal points two dimension unit (PLANE121). Table 1 shows the material property, unit type and setting of electric tension loading. The feature of plate-plate type is that metal plate is added to spinneret pipe, the metal plate is paralleled to negative plate, and the shape and size is the same as negative plate.

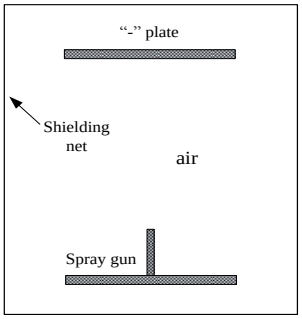

Figure 3. The Simplified FEA Model of Plate-plate Type

Table 1. Parameters Setting of the Model

Model	Spray gun	"-"plate	Air medium	Shielding net
Dielectric constant	2	2	1	5
Voltage load	10000V	-5000V	----	0V

3.3. Simulated Result of Electrostatic Field

In the electric field analysis of high-voltage electrostatic spinning, the distribution situation of electric field strength of electrostatic spinning should be considered. Figure 4 is vector distribution of nozzle on spinneret pipe of plate-plate type, and Figure 4 shows that the electric-field vector crosswise of electrostatic spinning electric field was axial symmetric distribution. Figure 4 also shows that: while the physical truth is the same, the maximum of field strength appeared on the position of spinning pipe orifice and its direction pointed upward vertical to the negative plate. The maximum of field strength was $E = 0.49 \times 10^6 V/m$. While the voltage is the same, the change of field strength E is caused by the change of area S. That is to say, while the surface area increases, the value of field strength E decreases. Figure 5 shows the relation between electric field and collecting distance of plate-plate type. We can find out that: the nearer the electric-field strength was to the negative plate, the faster the electric-field strength declined. The field strength sudden dropped to a lower value especially in a small distance near the spinneret pipe orifice.

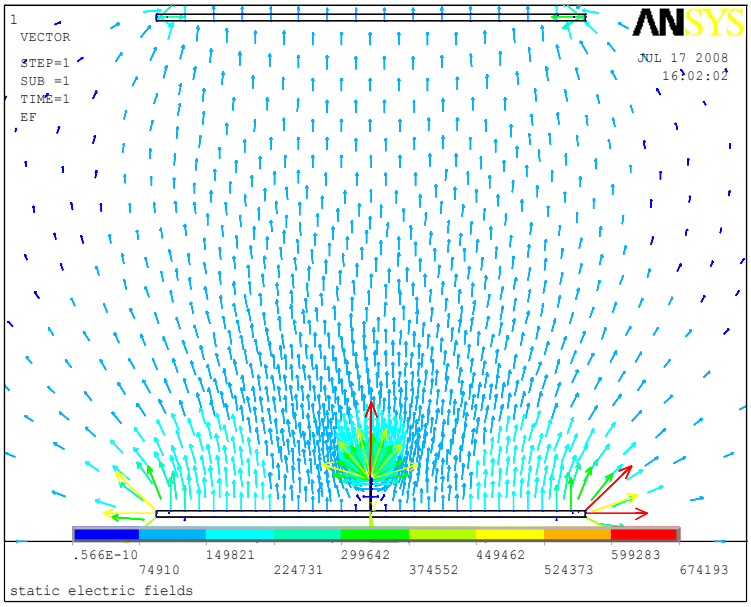

Figure 4 Vector Distribution of Nozzle on Spinneret Pipe of Plate-plate Type

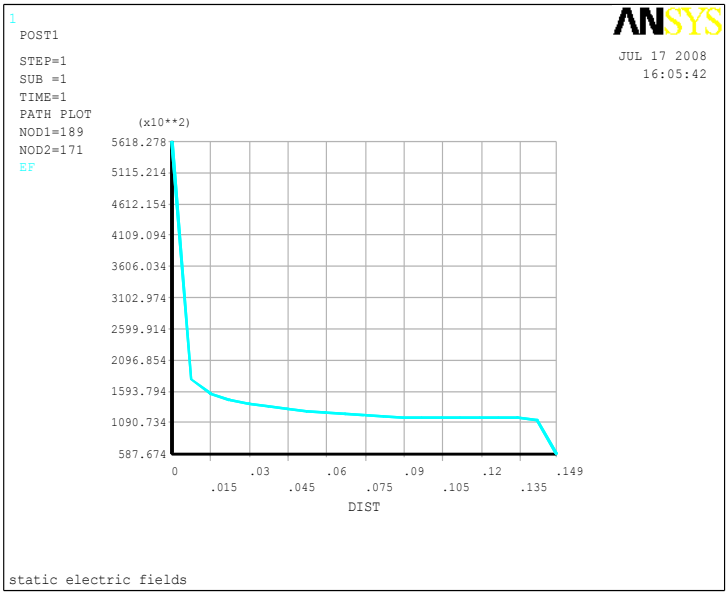

Figure 5. Relation between Electric Field and Collecting Distance of Plate-Plate Type

4. Electrospinning Experiment

4.1. Experimental System of the Electrospinning Machine

Experimental system of the electrospinning machine is shown in Fig. 6. High-voltage power supply, which is made of electrical department of Tsinghua University, can realize the continuous adjustment of the voltage in the range from 0V to 100KV. Shield mesh with uniform gap is weaved by metal wire. In order to reduce the interference of electric field to input signal, shielded cable is used as the connecting line between control platform and injection unit, between computer and control card.

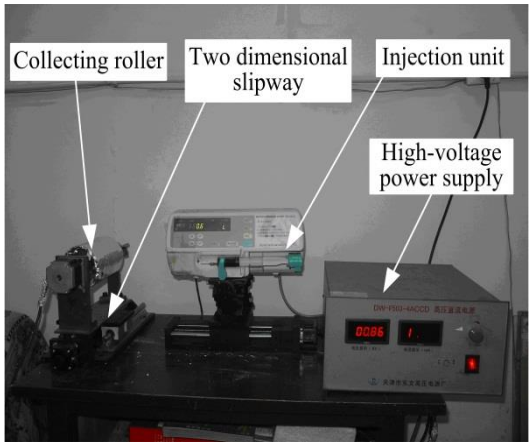

Figure 6. Experimental System of the Electrospinning Machine

4.2. Results and Analysis of Electrospinning Experiment with Different Spinning Distance

Electrospinning experiment with different spinning distance is performed using experimental system of the electrospinning machine. PAA solution concentration is 20wt%, the spinning voltage is 15KV, extrusion speed is 1.0ml/h, the rotation speed of the collection roller is 150RPM. We have tested polyimide nanofibers SEM images and fibers diameter respectively when the spinning distance is 16cm, 20cm and 24cm.

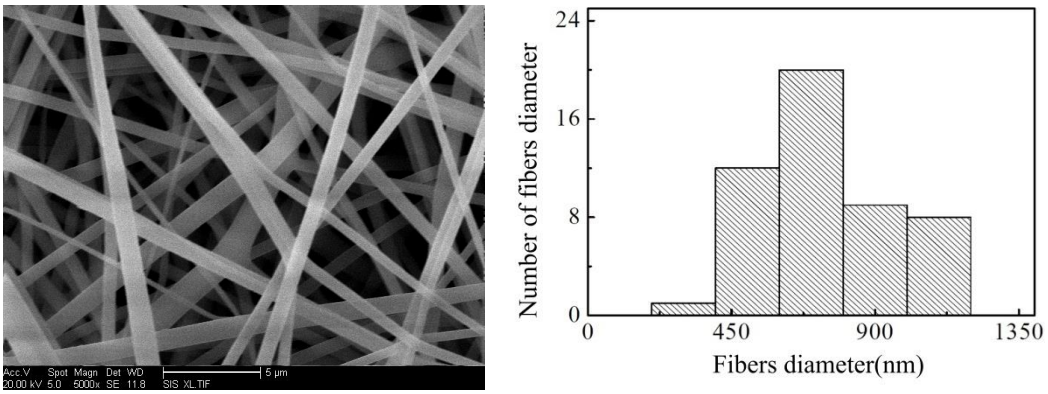

a) 16 cm

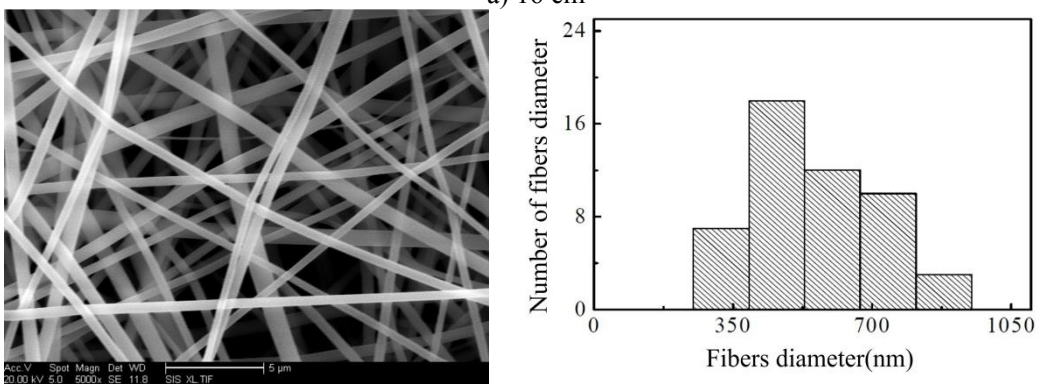

b) 20 cm

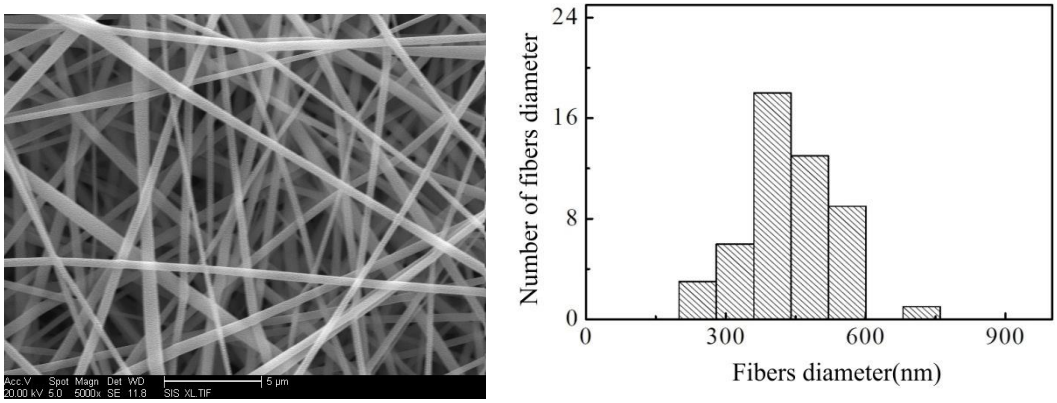

c) 24 cm

Figure 7. Polyimide Nanofibers SEM Images and Fibers Diameter Distribution Histogram with Different Spinning Distance

Figure 7 is polyimide nanofibers SEM images and fibers diameter distribution histogram with different spinning distance prepared by electrospinning machine. The magnification times of polyimide nanofibers SEM images are 5000 times. From the Figure 7, while the spinning distance increases from 16cm to 24cm, the diameter of polyimide nanofibers became fine obviously. From the fibers diameter distribution histogram, while the spinning distance is 16cm, the maximum number of nanofibers diameter is at 675nm. While the spinning distance is 20cm and 24cm, the maximum number of nanofibers diameter is at 500nm and 400nm respectively. From a theoretical point of view, while the spinning distance increases, the stretched and splitting procedure of nanofibers increases. So the increase of spinning distance will be beneficial to reduce the size of the fiber diameter. However, spinning distance is inversely proportional to the electrostatic field strength. Undoubtedly the increase of the spinning distance will reduce the field strength of electrostatic field, and thus reduce the electrostatic force. Then the decline of traction will lead to the increase of nanofiber diameter prepared by electrospinning machine. However, from Figure 7, we can see that fiber diameter decreases with the increase of spinning distance. In order to get the finer nanofibers, we can increase the spinning distance as far as possible.

Polyimide nanofibers' mean diameter and standard deviation with different spinning distance is as shown in Table 2. Figure 8 is nanofibers' mean diameter and standard deviation with different spinning distance.

Table 2. Fibers' Mean Diameter and Standard Deviation with Different Spinning Distance

Spinning distance (cm)	16	20	24
Fibers' mean diameter (nm)	775	555	437
Standard deviation (nm)	204	153	95

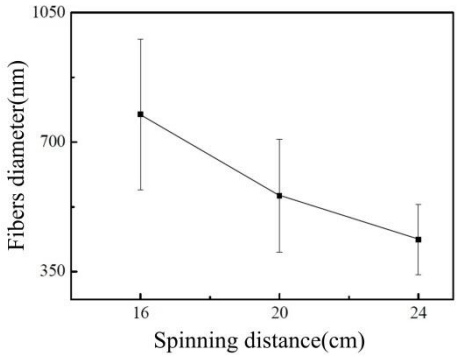

Figure 8. Fibers' Mean Diameter and Standard Deviation with Different Spinning Distances

From the data of Table 2 and Figure 8, while the spinning distance increase from 16cm to 20cm, polyimide nanofibers' mean diameter decrease from 775nm to 437nm, and standard deviation decrease from 204nm to 95nm. Reduction of fibers' diameter from 16cm to 20cm is superior to reduction of fibers' diameter from 20cm to 24cm. So, the increase of spinning distance can reduce the fiber' diameter, but the extent of decrease is not much. And while the fiber' mean diameter increase, the discrete degree of fibers' diameter distribution will increase.

4.3. Results and Analysis of Electrospinning Experiment with Different Extrusion Speed

Electrospinning experiment with different extrusion speed is performed using experimental system of the electrospinning machine. PAA solution concentration is 20wt%, the spinning voltage is 18KV, the spinning distance is 20cm, the rotation speed of the collection roller is 150RPM. We have tested polyimide nanofibers SEM images and fibers diameter respectively when the extrusion speed is 0.5ml/h, 1.0ml/h and 1.5ml/h.

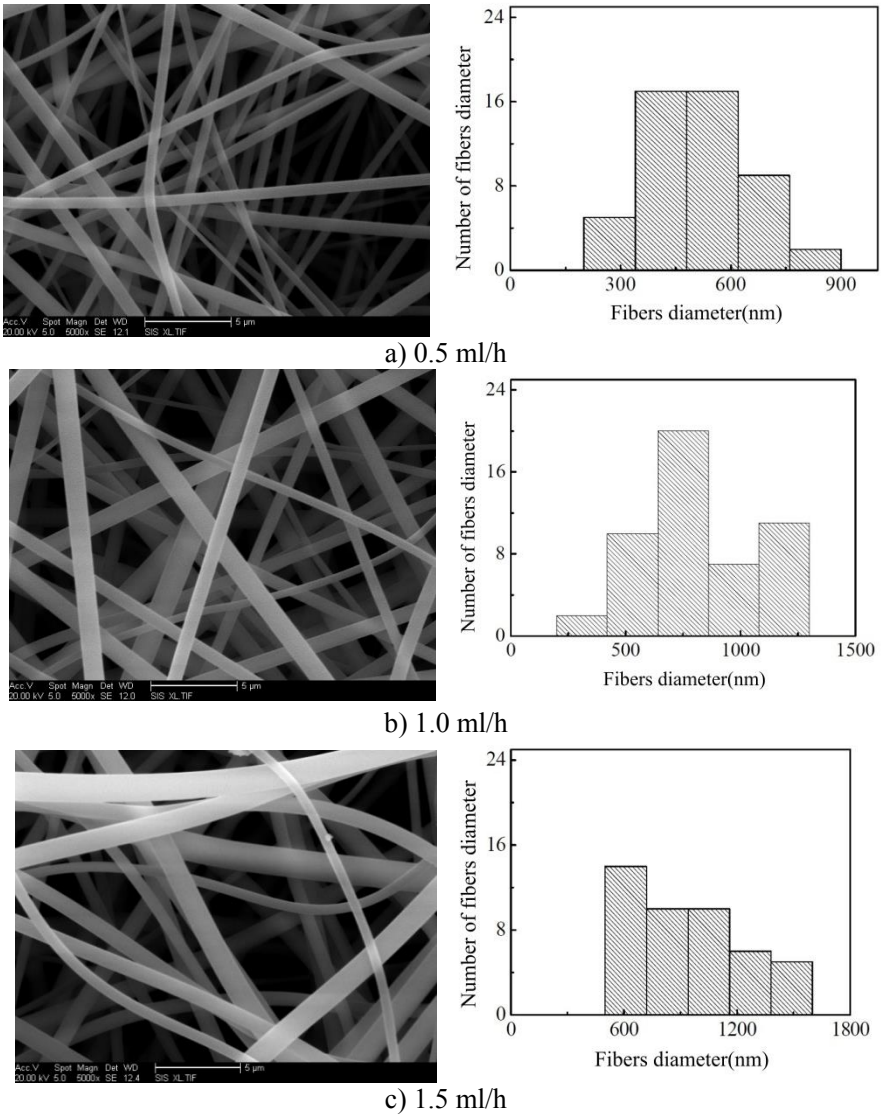

a) 0.5 ml/h

b) 1.0 ml/h

c) 1.5 ml/h

Figure 9. Polyimide Nanofibers SEM Images and Fibers Diameter Distribution Histogram with Different Extrusion Speed

Figure 9 is polyimide nanofibers SEM images and fibers diameter distribution histogram with different extrusion speed prepared by electrospinning machine. The magnification times of polyimide nanofibers SEM images are 5000 times.

In the process of electrospinning, the change of extrusion speed will directly affect the shape change of Taylor cone in nozzle of spinneret pipe. With the increase of the extrusion speed, Taylor cone becomes from small to big. The liquid drop on the nozzle of spinneret pipe is stretched gradually. When the extrusion speed increases, the fiber' extrusion amount of spinning solution in unit time will increase. And the magnitude of bending instability of the fiber will be lowered by the effect of gravity, so the final result is that this will affect the increasing of the diameter of the polyimide nanofibers. According to Figure 9, when the extrusion speed increases from 0.5ml/h to 1.5ml/h, there will be an obvious increase of the mean diameter of the nanofibers produced by electrospinning. According to the fibers diameter distribution histogram, the peak of the fiber's diameter obviously turns from subsize to jumbo size, when the extrusion speed is 1.5ml/h, the fiber whose diameter is smaller than 500nm cannot be obtained and the thickest fiber diameter almost reaches 1700nm.

Polyimide nanofibers' mean diameter and standard deviation with different extrusion speed is as shown in Table 3. Figure 10 is nanofibers' mean diameter and standard deviation with different extrusion speed.

Table 3. Fibers' Mean Diameter and Standard Deviation with Different Extrusion Speed

Extrusion speed (ml/h)	0.5	1.0	1.5
Fibers' mean diameter (nm)	520	795	1025
Standard deviation (nm)	134	244	359

From the data of Table 3, while the extrusion speed increases from 0.5ml/h to 1.5ml/h, polyimide nanofibers' mean diameter increase from 520nm to 1025nm. In Fig.10, it can be seen that the increase of the diameter of the fiber caused by the increase of the extrusion speed from 0.5ml/h to 1.0ml/h and from 1.0ml/h to 1.5ml/h is almost the same. It shows that the extrusion speed and the diameter of the fiber conform to the direct proportion. From the discrete degree of fibers' diameter distribution, it can be seen that the increase of the standard deviation also conforms to this rule. So it can be concluded that when the extrusion speed increase, the mean diameter of the fiber increases directly proportional and the discrete degree of the fiber' diameter distribution increases correspondingly at the same time, the distribution uniformity of the fiber' diameter reduces.

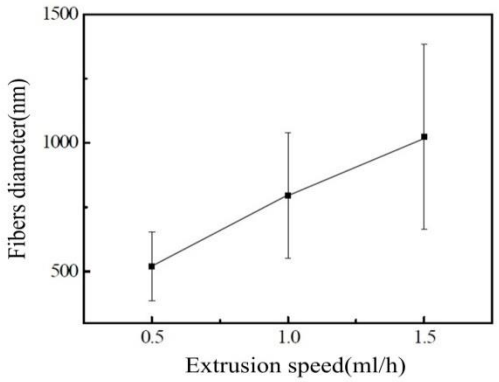

Figure 10. Fibers' Mean Diameter and Standard Deviation with Different Extrusion Speed

5. Conclusions

Electrospinning technique is currently one of the most important methods for preparing. It is important and essential to analyze the electric field distribution in electrospinning machine.

(1) Based on finite element calculation theory of electric field, electric field strength is calculated.

(2) Electric field structure of plate-plate type electrospinning machine is simulated using ANSYS software. And vector distribution of nozzle on spinneret pipe of plate-plate type electrospinning machine is obtained. The simulation analysis provides an effective reference for the electric field's distribution of the plate-plate type electrospinning machine.

(3) Based on the experimental system of the plate-plate type electrospinning machine, electrospinning experiment with different spinning distance and extrusion speed is performed. The experimentation results show that fiber diameter decreases with the increase of spinning distance, and the extrusion speed is proportional to the diameter of the fiber.

Acknowledgements

This research was supported by the Heilongjiang Postdoctoral Funds for Scientific Research Initiation (Grant No. LBH-Q13093) and Harbin Science and Technology Innovation Researchers Project (Grant No. 2012RFJGG013).

References

[1] K. An, H. Liu and S. Guo, "Preparation of Fish Gelatin and Fish Gelatin/poly(l-lactide) Nanofibers by Electrospinning", International Journal of Biological Macromolecules, vol. 47, no. 3, **(2010)**, pp.380-388.
[2] Z. Yuansheng and Z. Yongchun, "Electric Field Analysis of Spinneret Design for Multihole Electrospinning System", Journal of Materials Science, vol. 49, no. 5, **(2014)**, pp. 1964-1972.
[3] J. M. Deitzel, J. Kleinmeyer, D. Harris and N. C. Beck Tan, "The Effect of Processing Variables on the Morphology of Electrospun Nanofibers and Textiles", Polymer, vol. 42, no. 1, **(2001)**, pp. 261-272.
[4] S. Megelski and J. S. Stephens, "Micro and Nano-structrued Surface Morphology on Electrospun Polymer Fibers", Macro Molecules, vol. 35, **(2002)**, pp. 8456-8466.
[5] Y. Ying, J. Zhidong and L. Qiang, "A Shield Ring Enhanced Equilateral Hexagon Distributed Multi-needle Electrospinning Spinneret", IEEE Transactions on Dielectrics and Electrical Insulation, vol. 17, no. 5, **(2010)**, pp. 1592-1601.
[6] J. Jingang, H. Tianhua, D. Hongwei and L. Bin, "Electric Field Structure Analysis and Experimentation of Needle-plate Type Electrospinning Machine", International Journal of Control and Automation, vol. 7, no. 1, **(2014)**, pp. 369-378.
[7] Y. Enlongn and S. Jingjing, "Influence of Electric Field Interference on Three Nozzles Electrospinning", Advanced Materials Research, **(2011)**, pp. 189-193: 720-723.
[8] Z. Wenbing, S. Jingjing, H. Zhongming, Y. Pei and Y. Enlong, "Electric Field Simulation of Electrospinning with Auxiliary Electrode", Applied Informatics and Communication, vol. 288, no. 1, **(2011)**, pp.346-351.
[9] K. Okan, D. Mustafa, U. Tansel, C. Dilek and K. I. Cengiz, "An Alternative Electrospinning Approach with Varying Electric Field for 2-D-aligned Nanofibers", IEEE Transactions on Nanotechnology, vol. 13, no.1, **(2014)**, pp. 101-108.
[10] D. Hongwei and J. Jingang, "Experimentation and Finite Element Analysis of Electric Field Structure of Electrospinning Machine", Advances in Intelligent and Soft Computing, vol. 105, **(2011)**, pp. 283-289.
[11] J. Erol, G. Omer and O. Ertan, "A Comprehensive Electric Field Analysis of a Multifunctional Electrospinning Platform", Journal of Electrostatics, vol. 71, no. 3, **(2013)**, pp. 294-298.
[12] J. Angammana Chitral and H. Jayaram Shesha, "Investigation of the Optimum Electric Field for a Stable Electrospinning Process", IEEE Transactions on Industry Applications, vol. 48, no. 2, **(2012)**, pp. 808-815.